PHYSICAL REVIEW B VOLUME 25, NUMBER 1 1 JANUARY 1982

Electron-spectroscopy studies of clean thorium and uranium surfaces. Chemisorption and initial stages of reaction with O_2, CO, and CO_2

W. McLean, C. A. Colmenares, and R. L. Smith
Lawrence Livermore National Laboratory, Livermore, California 94550

G. A. Somorjai
Lawrence Berkeley Laboratory, University of California, Berkeley, California 94720

(Received 22 June 1981)

The adsorption of O_2, CO, and CO_2 on the thorium (111) crystal face and on polycrystalline α-uranium has been investigated by x-ray photoelectron spectroscopy, Auger electron spectroscopy (AES), and secondary-ion mass spectroscopy (SIMS) at 300 K. Oxygen adsorption on both metals resulted in the formation of the metal dioxide. CO and CO_2 adsorption on Th(111) produced species derived from atomic carbon and oxygen; the presence of molecular CO was also detected. Only atomic carbon and oxygen were observed on uranium. Elemental depth profiles by AES and SIMS indicated that the carbon produced by the dissociation of CO or CO_2 diffused into the bulk of the metals to form a carbide, while the oxygen remained on their surfaces as an oxide.

I. INTRODUCTION

Studies of the interaction of the actinide metals with reactive gases permits the investigation of the role of the $5f$ shells of electrons in chemical reactions. The $5f$ levels of the lighter actinides (i.e., thorium, uranium, and plutonium) are located near their respective Fermi levels, and are thought to overlap and hybridize with the partially filled $6d$ and $7s$ levels to form delocalized energy bands.[1,2] Thorium, with a valence-band structure of $5f^0 6d^2 7s^2$, has unoccupied $5f$ levels in the ground state approximately 3.15 and 4.5 eV above the Fermi level[3] and it is expected to exhibit properties similar to the fcc $5d$ metals[4] platinum and iridium. Uranium, with a $5f^3 6d^1 7s^2$ valence band, exhibits a high concentration of unoccupied $5f$ states just above the Fermi level which extend into the valence band.[3] Hence, uranium should display chemical properties mostly attributable to the influence of the $5f$ electrons. In sharp contrast to this behavior, the highly localized $4f$ levels of the rare-earth metals, with the exception of cerium, lie well below their $5d$ and $6s$ conduction bands and therefore do not affect the chemical properties of these metals.[5,6]

The intent of this investigation was to examine the chemisorption and initial stages of chemical reaction of O_2, CO, and CO_2 on clean thorium and uranium metals. Low-energy electron diffraction (LEED) studies on single crystals of thorium have indicated that adsorption of these gases at room temperature proceeds in a disordered manner.[7,8] We selected x-ray photoelectron spectroscopy (XPS) to probe the structure of adsorbed species through the study of the chemisorption of O_2, CO, and CO_2 on thorium and uranium from submonolayer to monolayer coverages at room temperature. Auger electron (AES) and secondary-ion mass (SIMS) spectroscopies were also used to clarify and confirm the behavior observed in the XPS studies.

Exposure of thorium and uranium to oxygen was observed to produce only metal dioxide in both cases. Carbon monoxide and dioxide dissociated on the surface of Th(111) at low coverages to produce carbon and oxygen. The former diffused into the metal to produce a carbide, while the latter remained on the surface as an oxide. "Graphitic" carbon and bound molecular CO were observed at high CO and CO_2 coverages, while a second molecular species, tentatively identified as a monodentate carbonate, was detected at saturation CO_2 coverage. Adsorption of CO and CO_2 on uranium was much simpler since each gas dissociated to produce carbon as a carbide below the surface and an oxide on the surface.

II. EXPERIMENTAL

A. Vacuum apparatus and procedures

Our experiments were performed in a stainless-steel vacuum chamber capable of obtaining a base

pressure of $\lesssim 3$ nPa (2×10^{-11} Torr). The chamber was evacuated by a 200 l/sec noble-ion pump, a water-cooled titanium sublimator, and a liquid-nitrogen trapped diffusion pump. The large capacity of the diffusion pump made it possible to maintain a flow of gases through the chamber during sample cleaning by inert gas ion bombardment or during exposure to active gases. This ensured that: (1) gaseous impurities generated during these operations were continuously swept out of the chamber, and (2) ultrahigh vacuum conditions were quickly restored after a given operation. It took one minute to evacuate the chamber from 6.7 mPa (5×10^{-5} Torr) to less than 13.3 nPa (1×10^{-10} Torr).

Research grade O_2, CO, and CO_2 were stored in one-liter stainless-steel cylinders at 1.4 MPa (200 psi). These flasks were connected directly to all-metal variable-leak valves to avoid the contamination problems encountered with regulators. Argon for sputter etching was stored and cleaned in a specially designed three-liter vessel that was first baked under vacuum at temperatures above 570 K. The interior surfaces were then coated with a thin calcium film using an internal evaporator operating at 920 K. The vessel walls were maintained at $\sim$370 K while filling with argon to prevent the formation of a protective oxide film on the calcium.[9] The calcium film gettered H_2O and O_2 to levels below 1 ppm under these conditions.

Carbon monoxide can account for up to 50% of the gas load in a clean ultrahigh vacuum (UHV) system during oxygen exposures in the presence of hot tungsten filaments.[7] Pretreatment of hot, thoriated iridium filaments in 0.13 mPa (1×10^{-6} Torr) oxygen for 20 minutes reduced the CO concentration to less than 1 vol% in oxygen at 6.7 μPa (5×10^{-8} Torr) while operating at low emission ($\sim$0.01 mA). It has also been demonstrated that many gases will interact with fresh titanium films in getter and/or ion-pump elements to release carbon monoxide, methane, and other uncontrolled contaminants[10]; for this reason, these pumps were isolated during active gas exposures.

B. Instrumentation

The Auger spectra displayed throughout this work were obtained with a scanning Auger microprobe (SAM) operating at a primary beam energy of 3 kV, a beam current of 5 μA, and a 6 V peak-to-peak modulation voltage in order to enhance the detection sensitivity to oxygen and carbon[11] while minimizing damage to the surface region. The modulation was reduced to 2 V peak-to-peak to improve the instrumental resolution when it was necessary to examine peak shapes in more detail.

The XPS measurments were made with nonmonochromatized Mg $K\alpha$ (1253.6 eV) radiation as an excitation source. A double pass cylindrical mirror analyzer (CMA) was used for electron-energy analysis. The CMA was operated in the retarding mode with a pass energy of 25 eV which gave Au $4f$ peaks with a full width at half maximum (FWHM) of 1 eV. The spectral features in the valence-band regions of both thorium and uranium were broad enough that we were able to obtain equal resolution with a pass energy of 50 eV as with 25 eV but in $\frac{1}{4}$ the time. The data were acquired in the pulse counting mode by taking multiple scans through the regions of interest in order to average out random noise. The number of sweeps ranged from 256 for strong peaks [O 1s, metal ($4f$)] to 1024 for weak peaks (C 1s). Spectra were normalized by factors determined by the average count rate in spectral regions with a flat background. Peak energies near the valence band were measured from a peak's center of gravity to the Fermi level. Peaks with higher binding energies were referenced to the Th $4f_{7/2}$ and U $4f_{7/2}$ levels at 333.1 and 377.2 eV, respectively.

Positive and negative secondary-ion mass spectra were taken to examine low-level impurities in the clean metals, and to resolve some of the interpretive problems raised by the AES and XPS results. These experiments utilized a 3-kV, 10-μA argon-ion beam excitation source with a 4$\times$4-mm raster on the sample.

III. MATERIALS AND SAMPLE PREPARATION

A 7-mm$^2\times$1-mm-thick sample of Th (111) was cut from a high purity, electrotransport-refined single crystal[12] and spot welded to a high purity thorium cap which was then fitted over a 50-W resistance heater. Use of the thorium cap prevented possible contamination of the sample by material sputtered from the molybdenum heater cover during cleaning; it also avoided alloying of the thorium crystal with molybdenum at elevated temperatures. A polycrystalline uranium sample, with a total impurity content of less than 100 ppm (Ref. 13) was mounted on a separate heater in a similar manner. W vs W$-$26 wt. % Re thermocouples were spot welded to each sample and used as tem-

perature monitors. Prior to installation in the argon filled vacuum chamber, the samples were etched in a 50 vol % solution of HNO_3 in H_2O to remove gross surface oxides, rinsed in distilled water and ethanol, and then dried under flowing argon.

We used the following cleaning procedure on new samples and on those that had undergone long term storage in the vacuum chamber:

(1) Clean by argon-ion bombardment [33.3 mPa (2.5×10^{-5} Torr), 5-kV beam voltage, 20-μA beam current, and 6×6 mm^2 raster] at room temperature until the oxygen *KLL* Auger signal is no longer detectable. (This operation requires from one to twenty-four hours.)

(2) Heat to 1073 K during argon sputtering until surface impurities are no longer detectable by AES.

(3) Stop sputtering and continue to anneal at 1073 K for 15 min.

(4) Let cool to room temperature.

(5) Repeat this procedure until oxygen can no longer be detected on the sample at room temperature. However, a significant amount of iron diffused to the surfaces of both thorium and uranium during this cooldown. Attempts to deplete the iron in the near surface region by repeated heat-cool-sputter cycles were unsuccessful. The surface iron was easily removed by sputtering for 30 sec at room temperature with a 0.5-kV argon-ion beam.

Recleaning between exposures was accomplished by approximately 30 sec of argon sputtering at 0.5 kV. It was necessary to repeat an abbreviated form of steps (1)—(5) whenever oxygen or carbon could not be removed easily.

The bulk impurities in thorium and uranium are listed in Table I. Most of the elements in this table were also found in our secondary-ion mass spectra. The major impurity species in thorium detected by SIMS were, in order of decreasing intensity: oxygen, fluorine, and aluminum. The dominant impurities in uranium were aluminum, silicon, and oxygen. None of these elements were present in amounts large enough to detect by AES or XPS.

AES is approximately an order of magnitude more sensitive to carbon and oxygen than XPS (Ref. 14); hence Auger spectra of these elements were taken at frequent intervals during XPS measurements on the clean metals to monitor surface cleanliness. The Auger spectrum in Fig. 1(a) is representative of the carbon and oxygen backgrounds on clean thorium. The carbon *KLL* peak is superimposed on the thorium O_1VV transition at 271 eV; however, the carbon contribution to the total peak height is not substantial based on the fact that the C^- peak in the secondary-ion mass spectrum was only 2% as large as the O^- peak under identical sputtering conditions. Since the relative sputter yield of carbon is roughly twice that of oxygen[15] and since oxygen could not be detected by AES, we concluded that the carbon content of the near surface region was negligible.

A clean thorium surface became contaminated by residual CO in the vacuum chamber during the 6 min it took to: (1) return to UHV conditions following sputter cleaning, (2) turn on the x-ray source, and (3) acquire a reasonable number of scans through one of the spectral regions (i.e., 128

TABLE I. Impurities in bulk samples of thorium and uranium.

Element	ppm in Th[a]	ppm in U[b]	Element	ppm in Th[a]	ppm in U[b]
Li	≤ 20	<0.2	K	50	0.06
B	≤ 10	0.06	Ca	700	0.2
C	~ 800	19	Sc	≤ 1	0.01
O	~ 1000	18	Ti	10	0.2
F	15	0.7	Cr	3	3.1
Na	250	0.03	Mn	1	7.7
Mg	25	11	Fe	25	12
Al		10	Co	≤ 5	0.05
Si		10	Ta	750	≤ 1.5
S	≤ 10	0.2	W	100	≤ 0.05
Cl	25	<10			

[a]Spark source mass spectrometric analysis.
[b]See Ref. 13.

for O 1*s*, C 1*s*, or Th 4*f*, 64 for the valence band). The increases in the (C + Th) and oxygen Auger signals are seen in Fig. 1(b). Comparison of the [O/Th] peak height in Fig. 1(b) with that from saturation CO coverage [Fig. 1(c)] led us to conclude that approximately 2% of a contamination monolayer had formed on the Th surface. This example represents the worst condition under which data collection was allowed to proceed. We were often unable to detect oxygen or carbon after 20–30 min in UHV; however, the spectra of the clean surfaces shown throughout this article were acquired in the 5-min interval immediately following recleaning of the sample. Recleaning and reexposure were performed at 5 min intervals to avoid contamination from background gases, especially at low coverage ($\leq \frac{1}{2}$ monolayer) of the active gases. CO contamination on thorium did not occur during oxygen exposure [Fig. 1(d)]. Similar recleaning procedures were followed for the uranium sample since it was also susceptible to rapid contamination by residual CO.

IV. RESULTS AND DISCUSSION

X-ray photoelectron spectra of thorium and uranium exposed to O_2, CO, and CO_2 will be presented and discussed in the following sections to illustrate the behavior of these gases after adsorption on the clean metals. The measurements on the thorium single crystal were repeated twice to ensure that the reported observations were consistent. The uranium spectra were reproduced on two different pieces of ultrapure uranium. The x-ray photoelectron spectra of clean thorium and uranium reflect the true signal-to-noise ratio of the experimental system; all other photoelectron spectra have been numerically smoothed.

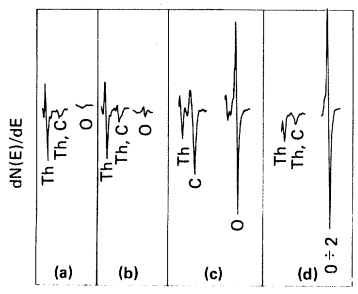

FIG. 1. Representative Auger spectra at various gas exposures: (a) clean thorium O_1VV; carbon KVV, and oxygen KVV background, (b) thorium after 5 min at 1×10^{-10} Torr, (c) Th + 10 L CO (1 L=0.13 mPa sec), (d) Th + 40 L O_2.

A. Valence band

Thorium

The valence-band regions (from −5 to + 45 eV) for clean thorium and for thorium at near saturation coverage for each of the gases under study are presented in Fig. 2. The three peaks in the clean thorium spectrum [Fig. 2(a)] originated from the $5f^06d^27s^2$, $6p_{3/2}$, and $6p_{1/2}$ electronic states corresponding to the Fermi level, 16.9 and 24.4 eV, respectively. The weak feature between 4 and 15 eV was thought to be due to the 2*p* levels of residual surface oxide. However, the intensity of this peak (referenced to the Th $6p_{3/2}$ peak) was ~37% of that for the O 2*p* on thorium at saturation O_2 coverage [Fig. 2(b)] and oxygen was not detected by AES or in the O 1*s* photoelectron spectrum. Hence the weak structure between 4 and 15 eV is most likely due to tailing of the Th $7s_{1/2}$ peak. The Th $6s_{1/2}$ at ~43 eV and the Th $5s_{1/2}$ at ~290 eV have approximately the same shape and breadth as the feature between 4 and 15 eV.

When thorium was exposed to O_2 a peak appeared between 4 and 9 eV, which we attributed to the unresolved O $2p_{3/2}$ and O $2p_{1/2}$ levels. The relationship between the decrease in the $6d^27s^2$ in-

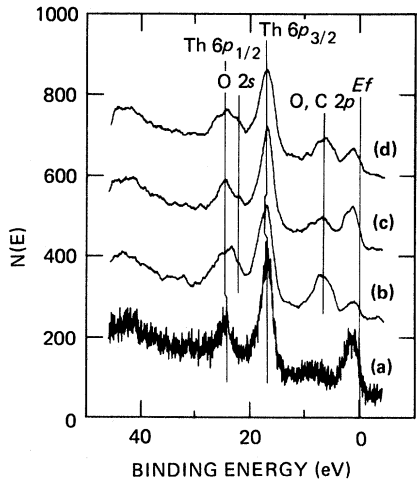

FIG. 2. Thorium valence-band region: (a) clean thorium, (b) Th + 40 L O_2, (c) Th + 10 L CO, (d) Th + 40 L CO_2.

tensity and the increase in the O $2p$ feature indicates that electrons were transferred from the valence band to the $2p$ levels of the oxygen ions in forming the metal-oxide bond. Changes observed in the thorium valence band as a function of oxygen exposure are correlated with changes in the (C $1s$ + O $1s$) intensities relative to the Th $4f_{7/2}$ peak and the changes in the (C $2p$ + O $2p$) intensities relative to the Th $6p_{3/2}$ peak in Table II. It was not possible to resolve the O $2s_{1/2}$ transition which appeared in the vicinity of the Th $6p_{1/2}$ level but we observed that the center of gravity of the Th $6p_{3/2}$ peak shifted to a higher binding energy (17.2 eV) after oxide formation.

The presence of a peak associated with the O $2p$ level has been used to distinguish dissociative from molecular adsorption of CO.[16] Appearance of this peak between 4 and 9 eV after CO adsorption on thorium [Fig. 2(c)] suggests that a surface oxide had formed subsequent to the dissociation of some of the CO molecules. Approximately 10% of the feature between 4 and 9 eV originated from C $2p$ electrons which can also appear in this binding energy range.[17] We were unable to determine whether any undissociated CO was present because the photoionization cross sections of the 5σ, 4π, and 4σ levels of CO were much smaller than those of other peaks in the valence-band region; this made them difficult to detect by XPS. Photoionization cross sections (Mg $K\alpha$ radiation) for selected levels of thorium and uranium and molecular CO are presented in Table III. The O $2s_{1/2}$ level at approximately 22.1 eV was almost resolved from the Th $6p_{1/2}$ level as shown in Fig. 2(c). The intensity of the Th $6d^2 7s^2$ peak decreased (Table II) by $\sim$22% on exposure to CO which indicates that not all of these electrons participated to form oxide or carbide bonds. The position and shape of the Th $6p_{3/2}$ remained unchanged. The O $2p$ and O $2s$ bands also appeared during CO_2 adsorption [Fig. 2(d)] which indicated that dissociation of the adsorbate had occurred. The intensity of the Th $6d^2 7s^2$ peak at the Fermi level decreased by 56% after adsorption of CO_2, nearly as much as that observed following saturation with exposure oxygen (Table II). At the same time, the centroid of the Th $6p_{3/2}$ peak shifted to 17.0 eV which indicated the formation of an oxide.

Uranium

The valence-band regions for clean uranium, and uranium at saturation coverage of O_2, CO, and CO_2 are illustrated in Fig. 3. The $5f^3 6d^1 7s^2$, $6p_{3/2}$, and $6p_{1/2}$ peaks from clean uranium [Fig. 3(a)] were found at the Fermi level, 17.4 and 26.8 eV, respectively. The asymmetry on the high binding energy side of the clean uranium $5f^3 6d^1 7s^2$ peak has also been observed in high resolution spectra[5]; it has been attributed to a combination of Gaussian and Lorentzian broadening due to instrumental and lifetime effects.[20] The tailing between 4 and 10 eV is most likely due to the U $7s_{1/2}$ level, which computational studies suggest should be a broad feature centered at about 3.5 eV.[21]

Examination of photoelectron peaks in the vicinity of the uranium valence band as well as in the U $4f$ region is complicated by the existence of multiple forms of the oxide, i.e., UO_2, UO_3, U_3O_8, and also by substoichiometric oxides such as UO which has been reported to form in the early stages of uranium oxidation.[22] The spectrum of uranium at saturation oxygen coverage [Fig. 3(b)] closely resembles that found for UO_2 (Ref. 23) and for UO_2 on uranium metal.[24] Observations by Beatham

TABLE II. Correlation of changes observed in the thorium valence band with oxygen exposure.

	$\left[\frac{\%\text{ decrease in thorium VB}}{I(\text{Th } 6p_{3/2})}\right]$	$\left[\frac{\%\text{ increase in } I(\text{C } 1s)+I(\text{O } 1s)}{I(\text{Th } 4f_{7/2})}\right]^a$	$\left[\frac{\%\text{ increase in } I(\text{O } 2p)+I(\text{C } 2p)}{I(\text{Th } 6p_{3/2})}\right]$
Species			
Th + 40 L O_2	74	71	58
Th + 100 L O_2	81	79[b]	79[b]
Th + 10 L CO	22	40	25
Th + 40 L CO_2	56	65	41

[a] I is the photoelectron intensities corrected by photoelectron cross sections.
[b] Normalized to % oxide $4f$ line present. See Sec. IV C.

TABLE III. Photoelectron cross sections for selected levels of thorium and uranium (Mg $K\alpha$ radiation).

Level	$\sigma \times 10^{22}$ (cm^2)[a]	Level	$\sigma \times 10^{22}$ (cm^2)	Level	$\sigma \times 10^{22}$ (cm^2)
Th $7s_{1/2}$	3.872	CO 5σ[b]	0.400	U $7s_{5/2}$	3.520
Th $6d_{5/2}$	9.812	CO 1π[b]	0.200	U $6d_{5/2}$	4.312
Th $6d_{3/2}$	6.952	CO 4σ[b]	1.000	U $6d_{3/2}$	3.124
Th $6p_{3/2}$	64.460	O $2p_{3/2}$	3.190	U $5f_{7/2}$	89.540
Th $6p_{1/2}$	23.540	O $2p_{1/2}$	1.606	U $5f_{3/2}$	71.280
Th $6s_{1/2}$	28.882	C $2p_{3/2}$	0.264	U $6p_{3/2}$	66.220
Th $5s_{1/2}$	121.220	C $2p_{1/2}$	0.132	U $6p_{1/2}$	23.320
		O $1s_{1/2}$	632.700		
		C $1s_{1/2}$	220.000		

[a]See Ref. 18.
[b]See Ref. 19.

et al.[23] and by Evans[25] on the change in photoelectron cross section with photon energy for the sharp peak of UO_2 at the Fermi level indicate that this peak is primarily of $5f$ character; hence bonding to oxygen is taking place mainly through the $6d$ and $7s$ electrons. Norton *et al.*[26] have reached a similar conclusion regarding the nature of the U $5f$ electrons in uranium nitride where binding occurred between the U $6d$ and N $2p$ electrons. We observed that the O $2p$ band for UO_2 appeared between 4 and 11 eV, and that the U $6p_{3/2}$ and U $6p_{1/2}$ peaks were shifted to the higher binding energies of 18.2 and ~28.9 eV, respectively. The O $2s$ peak was centered at about 24.2 eV.

Saturation adsorption of CO and CO_2 caused only minor changes in the valence-band region [Figs. 3(c) and 3(d)]; the most noticeable difference was a ~15% decrease in intensity of the $5f^3 7s^1 6d^2$ peak at the Fermi level after adsorption of either gas. There was also a faint suggestion of an additional feature around 24 eV due to an O $1s$ contribution. The photoionization cross sections for adsorbate levels were much smaller than those of neighboring uranium peaks (see Table III), making their observation by XPS difficult.

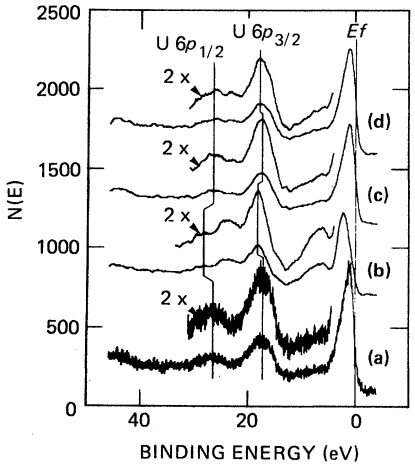

FIG. 3. Uranium valence-band region: (a) clean uranium, (b) U + 40 L O_2, (c) U + 10 L CO, (d) U + 40 L CO_2.

B. Carbon ($1s$) photoelectron peak and *KLL* Auger transitions

Thorium

The presence of the $5s$ level of thorium complicated the interpretation of spectral features in the C $1s$ region. This level appears as a diffuse (283 to 293 eV) low intensity peak [Fig. 4(a)] with a theoretical photoelectron cross section approximately one-half that of the C $1s$.[18] Relativistic Hartree-Fock calculations by Boring *et al.*[27] on thorium atoms indicate that the broad structure of the Th $5s$ level can be attributed to configuration interaction effects. Similar arguments have been applied to the shapes of the Th $5p$ levels[27,28]; the Th $5s$ peak of the oxidized metal was slightly narrower [Fig. 4(b)]. The carbon *KLL* Auger signal did not increase after O_2 exposure which provided verification that this was the metal oxide peak and not an effect of CO adsorbed from the residual gas [Fig. 1(d)]. The overlap of C $1s$ peaks with unspecifiable fractions of Th $5s$ metal and oxide levels made background subtraction in this region diffi-

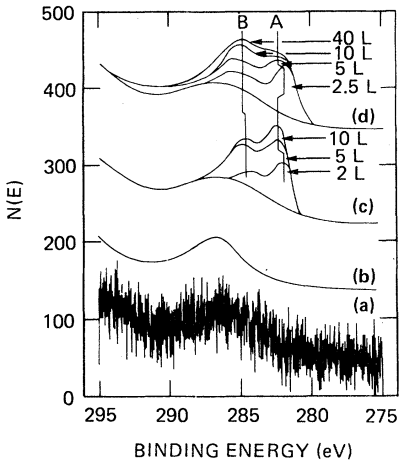

FIG. 4. Carbon 1*s* binding region on thorium: (a) clean thorium background, (b) Th + 40 L O_2, (c) Th + CO (exposures as marked), (d) Th + CO_2 (exposures as marked).

cult after CO and CO_2 exposures.

The evolution of several carbon species accompanied adsorption of CO. The first, labeled *A* in Fig. 4(c), appeared after an exposure of 2 L (1 L=0.13 mPa sec) and had a binding energy of 281.6±0.2 eV which is typical of many metal carbides.[29,30] Furthermore, the carbon *KLL* Auger peak at this low coverage [Fig. 5(b)] had the characteristic shape of a metal carbide with negative excursions at 255, 262, and 271 eV.[31–33] As the CO exposure was raised to 5 L [Fig. 4(c)] the centroid of the "carbidic" photoelectron peak shifted to 282.5±0.2 eV, while the carbon *KLL* peak began to assume a shape similar to that of graphitic carbon[33] [Fig. 5(c)] at approximately the same coverage (4 L). At even higher exposures ($\geq$5 L) another distinct form of carbon, labeled *B* in Fig. 4(c) appeared at a binding energy of 284.5±0.2 eV which falls within the range found for bound CO on a number of transition metals.[29,30,34] The carbon *KLL* Auger peak at saturation CO exposure [Fig. 5(d)] indicated the presence of both "carbidic" and "graphitic" carbon, and was decidedly different in shape from the lower coverage Auger peaks.

Exposure of clean thorium to increasing amounts of CO_2 yielded a similar family of C 1*s* peaks shown in [Fig. 4(d)]. A single carbon peak with a binding energy of 281.6 eV and a carbidic *KLL* Auger peak shape was observed at low exposure [Figs. 6(a) and 6(b)]. The shape of the carbon Auger peak changed dramatically at a CO_2 exposure of 10 L while a second feature, associated earlier with bound CO, appeared in the photoelectron spectrum at a binding energy of 284.5±0.2 eV [Fig. 4(d)]. This species was the dominant form of carbon at saturation CO_2 coverage. The carbon *KLL* Auger signal at this point [Fig. 6(d)] was almost 20 eV wide but had a peak-to-peak height smaller than that for a coverage of 6 L of CO_2. This observation illustrates the difficulty involved in obtaining quantitative information from Auger spectra of carbon compounds. The C 1*s* photoelectron spectrum of thorium at saturation CO_2 cover-

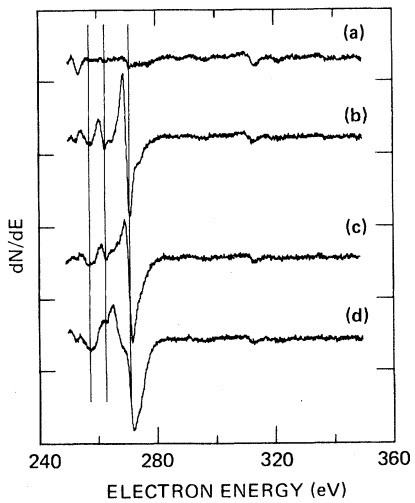

FIG. 5. Carbon *KLL* peak shapes for CO adsorption on thorium (a) clean thorium background, (b) Th + 2 L CO, (c) Th + 4 L CO, (d) Th + 10 L CO.

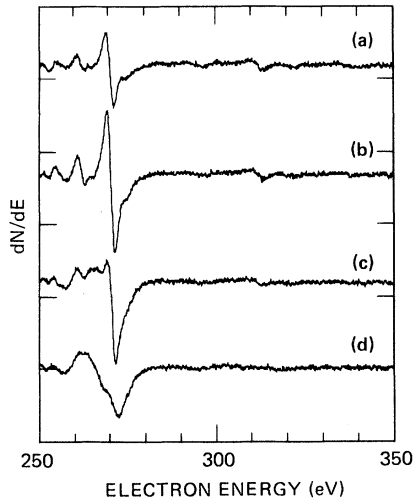

FIG. 6. Carbon *KLL* peak shapes for CO_2 adsorption on thorium: (a) Th + 3 L CO_2, (b) Th + 6 L CO_2, (c) Th + 10 L CO_2, (d) Th + 60 L CO_2.

age exactly duplicated the spectrum observed when a surface that had previously been covered to saturation with CO, was exposed to O_2

Uranium

The photoelectron spectrum of clean uranium in the C 1*s* region is not complicated by the presence of metal peaks [Fig. 7(a)]. Exposure to oxygen caused no changes in this region, proving that surface contamination by CO had not taken place [Fig. 7(b)]. Treatment of clean uranium with doses of CO up to 2000 L produced a single, asymmetric C 1*s* peak at 281.9 eV [Fig. 7(c)], close to the binding energy previously associated with a carbidic species on thorium; hence we concluded that this is a carbidic species on uranium as well. Confirmation of this assignment from the carbon *KLL* Auger peak shape was not possible because of interference from the uranium $N_6O_{4,5}P_{2,3}$, N_7O_4V, and $N_{6,7}O_{4,5}V$ transitions at 265, 271, and 280 eV, respectively.[35]

The asymmetry of the C 1*s* peak can be explained within the framework of the theoretical treatment of Schönhammer and Gunnarsson (SG model)[36] as a consequence of the formation of low-energy electron-hole pairs by promotion of electrons at the Fermi level to screening 5*f* levels immediately above E_F upon the sudden creation of a hole in the C 1*s* level. Fuggle *et al.* have reported many examples of similar adsorbate peak shape asymmetries[37] and have interpreted them in terms of the SG model and similar models proposed by Gumhalter[38,39] and Newns.[40] The asymmetry on the high-binding energy side of the C 1*s* peak for uranium at saturation CO_2 coverage [Fig. 7(d)] is much more pronounced than that for CO and may reveal the presence of a second adsorbed species. Infrared studies of CO_2 adsorbed on uranium oxide films have shown the existence of a strongly chemisorbed carboxylate species CO_2^-, which could not be removed at room temperature.[41] In our experiment, similar adsorption sites would be available to CO_2 molecules that reach the surface during the later stages of adsorption, when portions of the surface had already been oxidized.

C. Metal 4*f* levels

Thorium

Spectra of the 4*f* levels of clean thorium and thorium exposed to O_2, CO, and CO_2 are shown in Fig. 8. The 4*f* photoelectron spectrum for clean thorium is presented in Fig. 8(a). The small feature at approximately 325 eV (Fig. 8) is a satellite produced by the Mg $K\alpha_{3,4}$ radiation in the nonmonochromatized x-ray source. The shoulders on the high-binding-energy sides of the Th $4f_{7/2}$ and Th $4f_{5/2}$ peaks lie in positions deceptively close to where one would anticipate thorium oxide peaks to appear [Fig. 8(b)]. However, the area under these shoulders constitutes approximately 5% of the to-

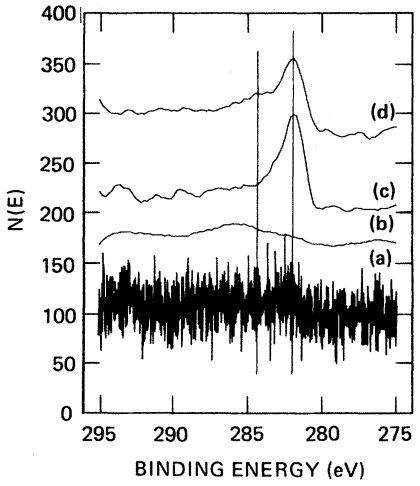

FIG. 7. Carbon (1*s*) binding region on uranium: (a) clean uranium, (b) U + 40 L O_2, (c) U + 10 L CO, (d) U + 40 L CO_2.

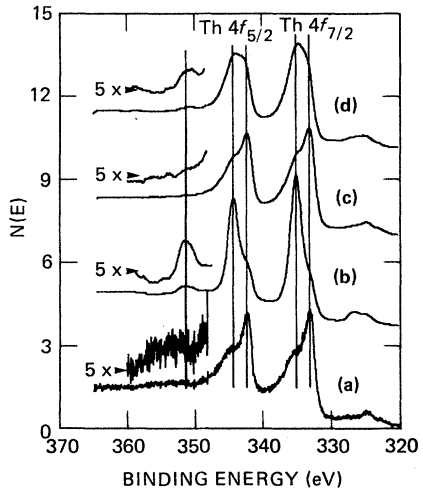

FIG. 8. Thorium (4*f*) peaks: (a) clean Th, (b) Th + 100 L O_2, (c) Th + 10 L CO, (d) Th + 40 L CO_2.

tal peak area, and it is difficult to believe that 5% surface oxide could not be detected either by XPS or by AES. An explanation for the origin of these shoulders has been advanced by Fuggle *et al.*[42] based on the SG model. Schönhammer and Gunnarsson[36] found that similar shoulders should result from the transfer of charge from the Fermi level to unoccupied screening levels which are pulled down below E_F upon creation of a hole in the highly localized core levels. Other important features of the model are coupling of the photoelectron to surface plasmons and configuration interaction effects. Schönhammer and Gunnarsson found that the shape of the satellite spectrum should be strongly dependent on the width of the screening level and on the amount of energy by which it is lowered after the ionizing event. Similar core-hole screening and configuration interaction effects have been observed in the 5*p* x-ray photoelectron spectrum of thorium[28] and in the 3*d* x-ray photoelectron spectra of the rare earths[43,44] and of nickel.[45]

The $4f_{7/2,5/2}$ peaks of oxidized thorium [Fig. 8(b)] were observed at binding energies of 335 and 344.3 eV, respectively. A Th $4f_{7/2}-$O $2p$ to valence-band (VB) shake-up satellite at ~343 eV is a contributing factor to the knee on the low-binding-energy side of the Th $4f_{5/2}$ peak. The Th $4f_{5/2}-$O $2p$ to VB shape-up satellite can be clearly seen at 351.7 eV. Satellites at these energies are characteristic of bulk ThO_2.[46,47] The knee on the low-binding-energy side of the oxidized Th $4f_{7/2}$ peak suggests the presence of unoxidized metal in the near surface region. An estimate of the metal contribution to the spectrum in Fig. 8(b) has been obtained by combining the spectra of the clean metal and the fully oxidized metal to yield the experimental spectrum. The results are presented in Fig. 9, where it is shown that 21% clean metal plus 79% oxide contribute to produce a spectrum that equals that of the clean metal exposed to 100 L oxygen. A spectrum of polycrystalline ThO_2 is shown in Fig. 9(d) for comparison.

The intensity of the Th $6d^27s^2$ level at the valence band for oxidized thorium [Fig. 2(b)] was greatly reduced as electrons from these levels became involved in metal-oxygen bonding. Hence the opportunity for carrying out charge transfer from levels near E_F to empty screening orbitals has been removed and the Th $4f_{7/2}$ level then assumes the symmetrical peak shape shown in Fig. 9(d) for a bulk oxide sample and in Fig. 9(b) for the oxide contribution to Fig. 8(b). The bulk oxide Th $4f_{5/2}$ line is still asymmetrical because of the presence of the Th $4f_{7/2}-$O $2p$ to VB shake-up line.

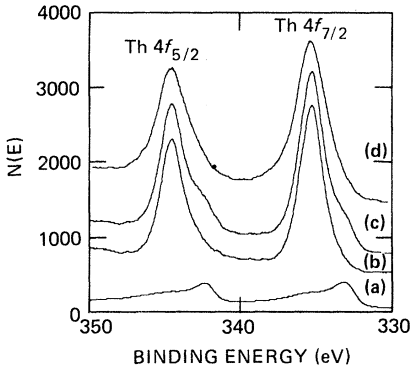

FIG. 9. Deconvolution of oxide contributions to Th $4f$ peaks: (a) 21% clean metal, (b) 79% oxide, (c) $a+b=$Th + 100 L O_2, (d) bulk oxide $4f$ lines.

The Th $4f$ levels at saturation coverage of CO are shown in Fig. 8(c). Since the changes observed here are not pronounced, especially on the scale of the illustration, they are presented in the form of a difference spectrum in Fig. 10(a) where it can be seen that the intensity of the clean metal lines at ~333 and ~342 eV decreased and the oxide lines at ~335 and ~344 eV increased. This is in agreement with observations in the valence band that indicated that some dissociation of CO and subsequent oxide formation had occurred. The areas above and below zero in the difference spectrum of Fig. 10(a), which represent intensity gained by the oxide and lost to the clean metal, are not equal for several reasons:

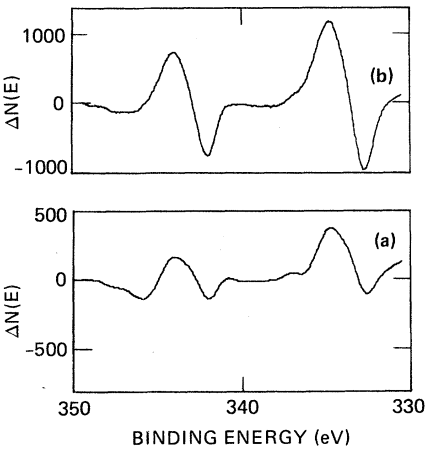

FIG. 10. Thorium ($4f$) difference spectra: (a) $4f$ (Th + 10 L CO)$-4f$ (clean Th), (b) $4f$ (Th + 40 L CO_2)$-4f$ (clean Th).

(1) the Th $4f$ peak shapes change from asymmetric in the metal to symmetric in the oxide;

(2) the Th $4f_{5/2}$ peak includes a Th $4f_{7/2}-$O $2p$ to VB shake-up transition;

(3) the inelastically scattered electron background changes shape when the metal converts to the metal oxide;

(4) the adsorbate introduces some attenuation of the Th $4f$ levels; and,

(5) the effect of core-hole screening changes as the population of the $6d^2 7s^2$ band at E_F decreases.

Since the changes in the Th $4f$ region were not as large as anticipated from the high intensity of the O $2p$ band near the valence band, it is possible that species other than ThO_2 (i.e., oxycarbides or chemisorbed oxygen) were formed after exposure of the clean metal to carbon monoxide.

The Th $4f$ levels at saturation CO_2 coverage are shown in Fig. 8(d). From the broadness of the peaks we deduced that both the clean metal and the oxide $4f$ lines were present. This became even more evident when we observed the difference spectrum in Fig. 10(b), where measurement of the areas under the curve revealed that the oxide was slightly more abundant than the metal. The comparison of relative intensities for the Th $4f_{5/2}$ peaks is obscured by the superposition of the ThO_2 shake-up line at 343.4 eV.[46] The Th $4f_{5/2}-$O $2p$ to VB shake-up satellite, typical of ThO_2, is clearly seen at 351.7 eV [Fig. 8(d)].

Uranium

The shapes of the clean uranium ($4f$) levels at 377.2 and 388.0 eV are reminiscent of the traditional Doniach-Sunjic[48] asymmetric line shape [Fig. 11(a)]. This line shape is also characteristic of the strong coupling limit of the SG model since the screening U $5f$ levels are not only delocalized,[1] but are located very close to E_F.[3] Uranium at saturation oxygen coverage [Fig. 11(b)] exhibited nearly symmetrical $4f_{7/2,5/2}$ peaks at 380.7 and 391.5 eV, respectively. However, $\sim$10% of the unoxidized metal $4f_{7/2}$ line was still visible at 377.2 eV. A satellite, observed approximately 7 eV above the U $4f_{5/2}$, was attributed to a shake-up transition from the oxygen derived $2p$ band to the now unoccupied $5f$'s at E_F. The residual metal $4f_{5/2}$ peak at 388.9 eV was distributed by the superposition of the U $4f_{7/2}-$O $2p$ to VB shake-up satellite at $\sim$381.5 eV. The positions of the

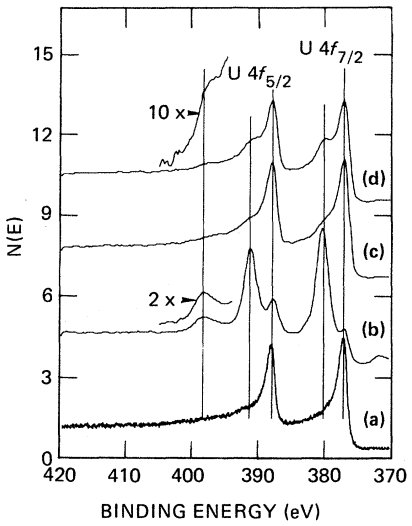

FIG. 11. Uranium $4f$ region: (a) clean uranium, (b) U + 40 L O_2, (c) U + 10 L CO, (d) U + 40 L CO_2.

oxide $4f$ peaks and of the shake-up satellites are very close to those found for bulk UO_2.[23,24,49]

Adsorption of CO and CO_2 on uranium [Figs. 11(c) and 11(d)] was followed by the appearance of small oxide shoulders on the high-binding-energy sides of the $4f_{7/2}$ and $4f_{5/2}$ peaks. The integrated intensities of the $4f_{7/2}$ peaks after adsorption of O_2, CO, and CO_2 were approximately 15 to 20% lower than the intensity of the clean uranium metal $4f_{7/2}$ peaks, even though the flat portions of the spectrum background between 415–420 eV and 370–375 eV contained the same numbers of counts. This loss of intensity, not observed for thorium under similar circumstances, was attributed to: (1) attenuation of the core line caused by scattering in the adsorbed atom[50]; (2) the filling of the 1.1- and 1.36-Å-diameter interstitial holes in the α-uranium surface by oxygen atoms, which precedes the rearrangement of the orthorhombic α-uranium to the fluorite UO_2 structure[51]; or (3) a combination of the above effects.

D. Oxygen ($1s$)

Thorium

The photoelectron spectrum of clean thorium between 520 and 540 eV is entirely structureless [Fig. 12(a)]. A single, symmetrical O $1s$ peak appeared at 531.0 eV [Fig. 12(b)] following increasing levels

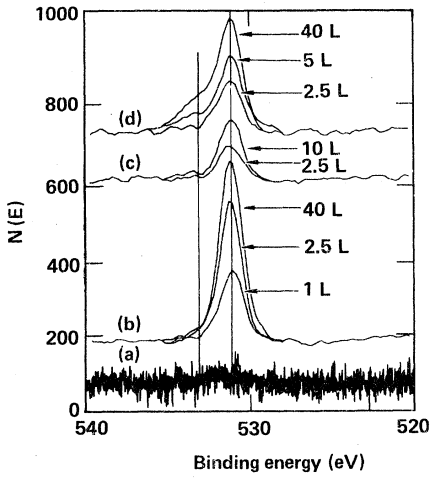

FIG. 12. Oxygen (1*s*) binding region on thorium: (a) clean thorium background, (b) Th + O_2 (exposures as marked), (c) Th + CO (exposures as marked), (d) Th + CO_2 (exposures as marked).

of O_2 exposure. Only a single O 1*s* line was observed after adsorption of CO [Fig. 12(c)] even though the results from the C 1*s* spectra suggested that bound CO was present. The experimentally determined oxygen binding energy is very close to the energy found for oxygen of bound CO on iron (100),[29] molybdenum,[30] nickel,[34] and ruthenium,[52] as well as for oxides of rare-earth metals.[53] We conclude that oxygen in CO is indistinguishable from oxygen on thorium. The fact that only one oxygen peak was observed rules out the possibility that the multiple C 1*s* peaks discussed in Sec. IV B are an artifact of adsorbate core-hole screening according to the SG model[54] or entirely a shake-up effect.[55] In either case we would have seen the same multiplicity in the O 1*s* peak as in the C 1*s* spectrum as has been observed for CO on Cu.[56] A small amount of a second oxygen species appeared at 533 eV for higher coverages of CO_2 [Fig. 12(d)]. Peaks associated with OH groups, formed by reactions of rare-earth metals with H_2O, have been observed at exactly this energy[53]; a similar shoulder on the high-binding-energy side of the O 1*s* peak on Ni (100) has been identified through SIMS analysis as an OH group.[57] However, it seems unlikely that OH groups would only appear during CO_2 exposures, since these were performed under the same conditions as O_2 and CO exposures. Furthermore, an increase in the intensity of the H_2O peak was not observed in the mass spectrum of the gas phase CO_2 under the exposure conditions.

ESR studies by Breysse *et al.*[58,59] have shown the existence of two forms of CO_2 bound to ThO_2: (1) a strongly bound monodentate carbonate where the carbon in CO_2 is bound to an oxygen atom on the ThO_2 surface; and (2) a weakly bound bidentate carbonate where the carbon in CO_2 is bound to a surface oxygen, while one of its oxygens is bound to a surface thorium. The latter configuration was found to be unstable in vacuum, but the monodentate carbonate was reported to be stable in vacuum to temperatures slightly below 770 K. The broad 4*f* lines observed for clean thorium plus CO_2 [Fig. 8(d)] indicate the formation of oxide sites which should be available for CO_2 adsorption during the later stages of our experiment. Hence we concluded that the 533-eV O 1*s* peak can be attributed to the carboxyl oxygen in a small amount of monodentate carbonate on the partially oxidized thorium surface.

Uranium

The O 1*s* regions for clean uranium and for uranium at saturation coverages of O_2, CO, and CO_2 are shown in Fig. 13. No structure was seen on the clean metal [Fig. 13(a)]. A single, slightly asymmetrical peak with a binding energy of 531.0 eV was detected following adsorption of each of the active gases [Figs. 13(b)—13(d)]. The asymmetry on the high-binding-energy side of the O 1*s* peak, induced by CO_2 adsorption [Fig. 13(d)], appeared to be slightly more pronounced than for the other gases. This observation reinforces our conclusion (Sec. IV B) that a second adsorbed species, possibly a carboxylate ion, exists on a partially oxidized uranium surface at high CO_2 coverages.

E. Peak position summary and quantitative analysis of oxygen and carbon

The binding energies of the thorium photoelectron peaks discussed in the previous sections are summarized in Table IV. These compare favorably with those from earlier studies on polycrystalline thorium films.[60] The energies of the carbon and oxygen species found at various exposures are summarized in Table V along with the amounts of carbon, oxygen, and thorium calculated to be present on the surface. Coverage calculations were based on the method of Wagner *et al.*[61] which makes use of the integrated intensities of the C 1*s*, O 1*s*, and Th $4f_{7/2}$ peaks normalized by corrections for in-

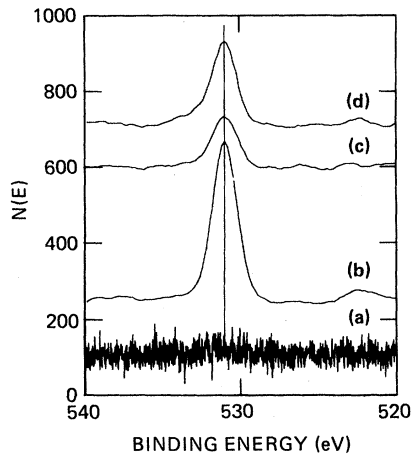

FIG. 13. Oxygen (1*s*) binding region on uranium: (a) clean uranium, (b) U + 40 L O_2, (c) U + 10 L CO, (d) U + 40 L CO_2.

strument sensitivity. These factors include the effects of the relative photoionization cross sections, electron escape depths and average take-off angle, and the analyzer transmission as a function of energy.

The most startling result of our coverage calculation was that for low coverages of CO and CO_2 the oxygen-to-carbon ratios are much higher than the [1/1] or [2/1] expected for adsorbed or dissociated CO and CO_2, respectively. The intensity of the C 1*s* peak was estimated by subtracting the clean Th 5*s* background from spectra with varying coverages of CO and CO_2. This subtraction procedure may have caused us to overestimate the C 1*s* intensity, because any oxide formation following decomposition of either adsorbate on the surface would result in changes in the Th 5*s* background intermediate between those shown in Figs. 4(a) and 4(b), i.e., an increase in the C 1*s* intensity. A second calculation which referred the amounts of carbon and oxygen to the clean metal $4f_{7/2}$ peak according to the method reported by Brundle,[29] also yielded excess oxygen in the surface region. Considering the assumptions we applied to the analytical techniques used and the poor signal-to-noise ratio, particularly for the C 1*s* line, we did not expect to obtain exact coverages but would expect the ratio [O/C] to reflect those of the near surface region within $\pm 10\%$.[29,34] Assuming that carbon was not lost to the gas phase, we concluded that free carbon produced by the dissociation of CO or CO_2 had dissolved into the bulk of the thorium crystal. We will discuss experimental evidence in support of this statement in the next section.

The photoelectron binding energies of the uranium, carbon, and oxygen levels discussed in the previous sections are summarized in Table VI. The mole fractions of carbon, oxygen, and uranium for saturation coverages of O_2, CO, and CO_2 in the surface region are listed in Table VII. The [O/C] ratios were larger for uranium at saturation CO and CO_2 coverages than the [1/1] or [2/1] expected for the simple chemisorption of these gases, respectively. In both cases, the excess of oxygen suggests that carbon, liberated upon dissociation of either molecule, had penetrated the uranium lattice, leaving the oxygen behind on the surface.

F. Depth profiles of exposed thorium and uranium samples

To determine the fate of carbon after adsorption of CO and CO_2, elemental depth profiles of the surface region were carried out by AES (oxygen, carbon, and thorium) and SIMS (C^- and O^-) using argon ions (3 kV, 10 μA, 4×4 mm^2 raster). The peak-to-peak heights of the oxygen-*KLL*,

TABLE IV. Photoelectron binding energies for selected thorium levels.

	Binding energy (eV)					
Condition	Th $6p_{3/2}$	Th $6p_{1/2}$	Th $5s_{1/2}$	Th $4f_{7/2}$	Th $4f_{5/2}$	Th $4f_{5/2}-O\,2p$ to VB satellite
Clean	16.9	24.4	280–292	333.1	342.3	
+ 40-L O_2	17.2	a	282–290	335.0	344.3	351.7 eV
+ 10-L CO_2	17.0	24.6	a	333.1	342.3	
+ 40-L CO_2	17.0	24.5	a	b	b	351.7 eV

[a]Deconvolution required.
[b]Both species present in roughly equal amounts.

TABLE V. Carbon and oxygen (1*s*) binding energies and quantitative analysis of these elements as a function of exposure of thorium (111).

Gas	Exposure (L)[a]	Binding energy (eV) C 1*sA*[b]	C 1*sB*[b]	O 1*sA*	O 1*sB*	Mole fraction O	C	Th	Atomic ratio [O/C]	[O/Th]
O_2	40			531.0		0.57		0.43		1.3
Bulk ThO_2 sample[c]				531.0		0.60		0.40		1.5
CO	2	281.7		531.0		0.14	0.10	0.76	1.4	0.18
CO	5	282.2	284.3	531.0		0.22	0.16	0.62	1.4	0.35
CO	10	282.2	284.3	531.0		0.21	0.18	0.61	1.2	0.35
CO_2	5	281.8	284.6	531.0		0.32	0.12	0.56	2.6	0.57
CO_2	10	282.2	284.4	531.0	533.0	0.34	0.12	0.54	2.9	0.63
CO_2	20	282.8	284.5	531.0	533.0	0.41	0.14	0.44	2.9	0.93
CO_2	30	282.6	284.4	531.0	533.0	0.41	0.13	0.46	3.1	0.89

[a]1 L=0.13 mPa sec.
[b]See Fig. 4.
[c]Polycrystalline sample on gold substrate.

thorium-N_7O_5V, and carbon-*KLL* Auger signals were plotted as a function of sputtering time in Fig. 14 for the thorium sample at saturation CO coverage. The oxygen signal disappeared in approximately 1 min, whereas the carbon signal exhibited an initial rise and then decreased very slowly. This initial increase in the carbon signal was not a true indication of a high concentration of subsurface carbon; rather it reflected the increase in peak-to-peak height in progressing from surface graphitic carbon to the carbidic form. This can be visualized by following the reverse of the sequence presented in Fig. 5. The significant result is that carbon was detectable long after all of the oxygen was removed, even though the relative sputter yield for carbon is approximately twice that for oxygen,[15] indicating that carbon had penetrated deeper into the thorium lattice than had oxygen. Additional evidence for this phenomenon is presented in Fig. 15, where the intensities of the O^- and C^- peaks in the secondary-ion mass spectra were recorded while the depth profile of Fig. 14 was being taken. The C^- ion intensity increased to a maximum and then slowly decreased to its background level over a period of 30 min. Oxygen, on the other hand, was reduced to its background level in about four minutes. *Similar behavior was observed in depth profiles for thorium at saturation* CO_2 *coverage, and for uranium samples covered with either* CO *or* CO_2.

V. REACTION MECHANISM

Thorium

The evidence presented in Sec. IV allows us to propose mechanisms for the interaction of O_2, CO, and CO_2 with clean thorium at room temperature. Because oxygen adsorption was accompanied by the immediate shift of the Th 4*f* lines to higher binding energies and by the development of ThO_2

TABLE VI. Photoelectron binding energies for U, C, and O as a function of adsorbate.

Surface condition	Binding energy (eV) U $6p_{3/2}$	U $6p_{1/2}$	U $4f_{7/2}$	U $4f_{5/2}$	U $4f_{5/2}$–O 2*p* to VB satellite	C 1*s*	O 1*s*
Clean	17.4	26.8	377.2	388.0			
Saturation O_2	18.2	28.9	380.7	391.5	398.5		531.0
Saturation CO	17.4	26.5	377.2	388.0		281.9	531.0
Saturation CO_2	17.5	26.5	377.2	388.0	398.5	281.9	531.0

TABLE VII. Quantitative analysis of uranium near the surface region.

Surface condition at saturation	Mole fraction O	C	U	Atomic ratio [O/C]	[O/U]
O_2	0.64		0.36		1.8
CO	0.29	0.14	0.57	2.1	0.5
CO_2	0.43	0.14	0.43	3.1	1.0

shake-up satellites, we concluded that oxidation of the metal rather than chemisorption was taking place.[62] This is consistent with the observations of Rivière[63] that oxygen atoms, formed from dissociated O_2, easily penetrate the 2 Å diameter interstitial holes present in cubic thorium to form the ThO_2 fluorite structure. Presence of the metal Th $4f_{7/2}$ line at very high oxygen exposures implied that either the oxide layer formed was not very thick or that oxide formation was proceeding by an island growth mechanism; thorium oxidation studies by LEED (Refs. 7 and 8) suggest the latter to be the case.

The reaction mechanisms for CO and CO_2 adsorption are not as straight forward. The interaction of CO with thorium is postulated to follow the sequence of steps illustrated in Fig. 16, assuming that the O 1*s* levels from the metal oxide and from bound CO have approximately the same binding energies and are indistinguishable. Adsorption of CO molecules on the clean metal takes

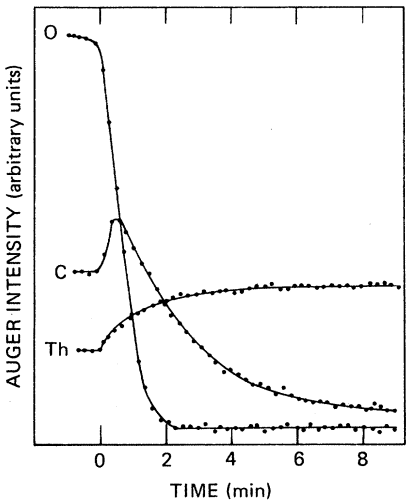

FIG. 14. AES elemental depth profile of Th + 10 L CO.

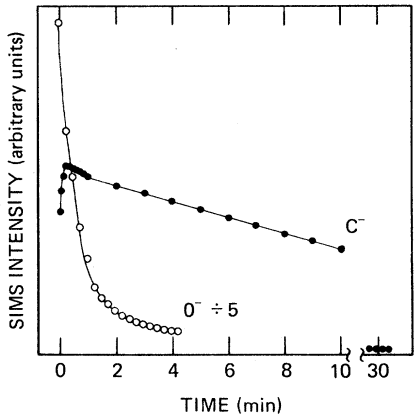

FIG. 15. C^- and O^- secondary-ion intensity as a function of time.

place via a linear carbon-to-metal bond as shown in step 16(a). The molecule then becomes bound to two metal atoms in step 16(b). This configuration is short lived and the carbon-oxygen bond is broken in step 16(c). The thermodynamic criterion governing CO dissociation on metals rests on the ability of the metal to form a stable carbide,[64] as is the case with thorium.[65] Carbon produced in steps 16(a)—16(c) diffuses into the thorium lattice as shown in steps 16(d) and 16(e), resulting in the "carbide" peak presented in Figs. 4(c) and 5(b). The shift in the C 1*s* binding energy and the change in the carbon *KVV* Auger peak shape to a more graphitic form [Figs. 3(c) and 4(d)] may be explained by the existence of an energetically different carbon C#, which might result from a

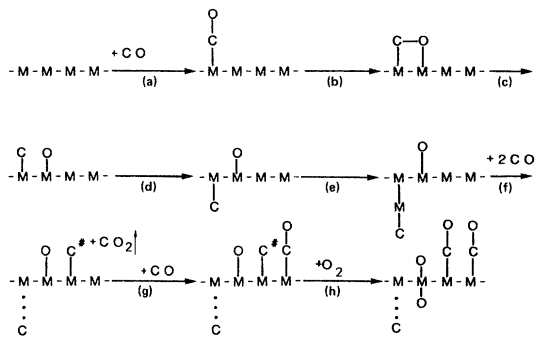

FIG. 16. Adsorption mechanism for CO on thorium. Steps (a)—(h) described in text.

Boudouard reaction [Fig. 16, step (f)]. Once coverage reaches approximately $\frac{1}{2}$ monolayer, the probability of a CO molecule landing on a site with vacant nearest neighbors is decreased, so that the adsorbed CO molecules cannot dissociate as per steps 16(a)—16(f); hence we begin to see molecularly bound CO in step 16(g). Support for this step is provided by the 284.5 eV C 1*s* peak in Fig. 4(c). Although not shown here, our experiments have shown that exposure of the CO treated surface to O_2 converts most of the free carbon on the surface to bound CO.

A more elaborate reaction sequence is needed to explain the spectral features encountered during the adsorption of CO_2 on thorium (Fig. 17). In step 17(a) linear CO_2 is adsorbed on the metal, followed in 17(b) by the breaking of the C—O bonds as evidenced by the carbidic photoelectron and Auger peaks in Figs. 4(d) and 6(a). During the initial stages of adsorption the [O/C] ratio was much greater than 2.0, which suggests that in this case free carbon also dissolved into the thorium lattice to form a carbide [step 17(c)]. This assertion was experimentally verified by AES depth profiles (Sec. IV F). Adsorption that involves binding of the carbon in CO_2 to a metal atom [step 17(d)] could result in either complete dissociation as shown in step 17(e) or in partial dissociation yielding a bound CO molecule as in step 17(f). An atomic arrangement similar to 17(f) is thought to occur following CO_2 adsorption on tungsten,[66,67] and would account for the similarity in binding energy for the 284.5 eV C 1*s* peak [Fig. 4(d)] to that of bound CO. The analogous adsorption over an oxygen site would lead to the formation of the monodentate carbonate of step 17(g), which is known to exist for CO_2 on thoria[58,59] and could account for the second oxygen peak at 533 eV [Fig. 12(d)].

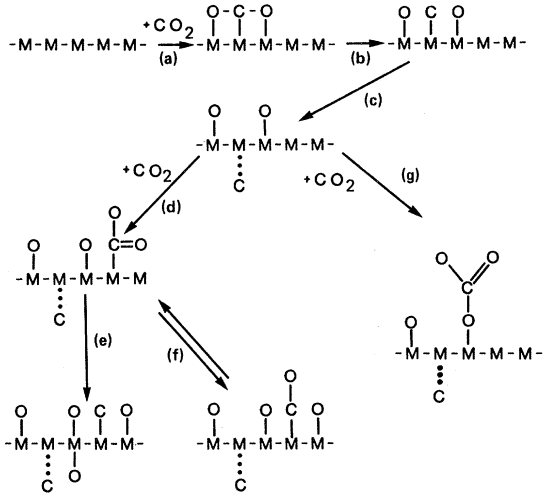

FIG. 17. Adsorption mechanism for CO_2 on thorium. Steps (a)—(g) described in text.

Uranium

The adsorption of O_2, CO, and CO_2 on uranium does not exhibit as many structural features as were observed for adsorption on thorium. Adsorption of oxygen led to the formation of a surface oxide with an approximate stoichiometry of $UO_{1.8}$ with a spectrum similar to bulk UO_2's. The low [O/U] ratio observed experimentally was due to incomplete oxidation of the near surface region, as can be seen in the clean metal line that accounts for 10% of the intensity in Fig. 11(b). It is not yet possible to speculate whether oxidation is proceeding by an island growth mechanism similar to the oxidation of thorium in the absence of LEED data from single-crystal samples. Since the reactions of uranium with both CO and CO_2 yielded only single carbon and oxygen species, it appears that adsorption of these gases was either completely dissociative or produced only bound CO and oxide similar to the structure postulated earlier [Figs. 16(g) or 17(f)]. Conclusive evidence in support of either scheme must await further experimentation with other techniques.

VI. CONCLUSIONS

We found that the reactions of O_2, CO, and CO_2 with clean thorium and uranium surfaces at room temperature exhibit a remarkable similarity to the interactions of these same gases with *d*-band transition metals. Oxide formation on both thorium and uranium proceeded by the transfer of 6*d* electrons from the metal to the oxygen 2*p* levels. Uranium has a high concentration of 5*f* states in its valence band while thorium does not. Thorium partially dissociated CO and CO_2 leaving a mixture of metal oxide, metal carbide, and bound CO in the near surface region. A small amount of a monodentate carbonate species was also observed in the later stages of CO_2 adsorption. Adsorption of CO and CO_2 on uranium took place in a totally dissociative manner, although in the later stages of CO_2 ad-

sorption a second bound species was also observed and identified as a carboxylate species. Many-body effects and core-hole screening in the photoelectron emission process on both metals played a strong role in determining the line shapes of the core levels.

ACKNOWLEDGMENTS

This work was performed under the auspices of the U. S. Department of Energy at the Lawrence Livermore National Laboratory under Contract No. W-7405-ENG-48.

[1]A. J. Freeman, in *Rare Earths and Actinides, 1977,* edited by W. D. Conner and B. K. Tanner (Institute of Physics, London, 1978), Vol. 37, p. 120.
[2]A. J. Freeman and D. D. Koelling, in *The Actinides: Electronic Structure and Related Properties,* edited by A. J. Freeman and J. R. Darby, Jr. (Academic, New York, 1974), Chap. 2.
[3]Y. Baer and J. K. Lang, Phys. Rev. B 21, 2060 (1980).
[4]J. H. Weaver and C. G. Olsen, Phys. Rev. B 15, 4602 (1977).
[5]J. K. Lang, Y. Baer, and P. A. Cox, Phys. Rev. Lett. 42, 74 (1978).
[6]J. K. Lang, Y. Baer, and P. A. Cox, J. Phys. F 11, 121 (1981).
[7]T. N. Taylor, C. A. Colmenares, R. L. Smith, and G. A. Somorjai, Surf. Sci. 54, 317 (1976).
[8]R. Bastasz, C. A. Colmenares, R. L. Smith, and G. A. Somorjai, Surf. Sci. 67, 45 (1977).
[9]D. A. Nissen, Oxid. Met. 11, 241 (1977).
[10]J. J. Quinn and R. B. Elliot, Vacuum 27, 473 (1977).
[11]L. E. Davis, N. C. MacDonald, P. W. Palmberg, G. E. Riach, and R. G. Weber, *Handbook of Auger Electron Spectroscopy,* 2nd ed. (Physical Electronics, Inc., Eden Prarie, MN, 1976).
[12]Obtained from D. T. Peterson, Iowa State University, Ames, IA. See D. T. Peterson and F. A. Schmidt, J. Less-Common Met. 24, 233 (1971).
[13]Obtained from G. L. Powell, Union Carbide Corp., Y-12 Plant, Oak Ridge, TN. See G. L. Powell and J. B. Condon, Anal. Chem. 45, 2349 (1973).
[14]L. J. Brillson and G. P. Caesar, J. Appl. Phys. 47, 4195 (1976).
[15]G. R. Sparrow, presented at the 25th Annual Conference on Mass Spectroscopy and Allied Topics, Washington, D. C., 1977.
[16]T. N. Rhodin and C. F. Brucker, Solid State Commun. 23, 275 (1977).
[17]G. Brodén, T. N. Rhodin, C. Brucker, R. Benbow, and Z. Hurych, Surf. Sci. 59, 593 (1976).
[18]J. H. Scofield, J. Electron. Spectrosc. 8, 129 (1976).
[19]J. W. Rabalais, *Principles of Ultraviolet Photoelectron Spectroscopy* (Wiley, New York, 1977), p. 104.
[20]Y. Baer, Physica B 102, 104 (1980).
[21]D. D. Koelling and A. J. Freeman, Phys. Rev. B 7, 4454 (1973).
[22]L. Leibowitz, J. G. Schnizlein, J. D. Bingle, and C. Vogel, J. Electrochem. Soc. 108, 1155 (1961).
[23]N. Beatham, A. F. Orchard, and G. Thorton, J. Electron. Spectrosc. 19, 205 (1980).
[24]J. Verbist, J. Riga, J. J. Pireaux, and R. Caudano, J. Electron. Spectrosc. 5, 193 (1974).
[25]S. Evans, J. Chem. Soc. Faraday Trans. 2 73, 1341 (1977).
[26]P. R. Norton, R. L. Tapping, D. K. Creber, and W. J. L. Buyers, Phys. Rev. B 21, 2572 (1980).
[27]M. Boring, R. D. Cowan, and R. L. Martin, Phys. Rev. B 23, 445 (1981).
[28]T. K. Sham and G. Wendin, Phys. Rev. Lett. 44, 817 (1980).
[29]C. R. Brundle, IBM J. Res. Develop. 22, 235 (1978).
[30]S. J. Atkinson, C. R. Brundle, and M. W. Roberts, Chem. Phys. Lett. 24, 175 (1974).
[31]H. P. Bonzel and H. J. Krebs, Surf. Sci. 91, 499 (1980).
[32]D. W. Goodman and J. M. White, Surf. Sci. 90, 201 (1979).
[33]D. W. Goodman, R. D. Kelley, T. E. Madey, and J. T. Yates, J. Catal. 63, 226 (1980).
[34]T. Fleisch, G. L. Ott, W. N. Delgass, and N. Winograd, Surf. Sci. 81, 1 (1979).
[35]Tentative assignments based on binding energies from Ref. 60 and δ values from W. P. Ellis, Surf. Sci. 61, 37 (1976).
[36]K. Schönhammer and O. Gunnarsson, Surf. Sci. 89, 575 (1979), and references therein.
[37]J. C. Fuggle, E. Umbach, D. Menzel, K. Wandelt, and C. R. Brundle, Solid State Commun. 27, 65 (1978).
[38]B. Gumhalter, Surf. Sci. 80, 459 (1979).
[39]B. Gumhalter, J. Phys. C 10, L219 (1977).
[40]B. Gumhalter and D. M. Newns, Phys. Lett. 53A, 137 (1975).
[41]C. Colmenares, J. Phys. Chem. 78, 2117 (1974).
[42]J. C. Fuggle, M. Campagna, Z. Zolnierek, R. Lässer, and A. Platau, Phys. Rev. Lett. 45, 1597 (1980).
[43]G. K. Wertheim and M. Capagna, Solid State Commun. 26, 553 (1978).
[44]G. Crecelius, G. K. Wertheim, and D. N. E. Buchanan, Phys. Rev. B 18, 6519 (1978).
[45](a) S. Hüfner and G. K. Wertheim, Phys. Lett. 51A, 299 (1975); (b) 51A, 301 (1975).
[46]J. J. Pireaux, J. Riga, C. Thibaut, C. Tenret-Noël, R. Caudano, and J. J. Verbist, Chem. Phys. 22, 113 (1977).
[47]G. M. Bancroft, T. K. Sham, J. L. Esquivel, and S. Larsson, Chem. Phys. Lett. 51, 105 (1977).
[48]S. Doniach and M. Šunjić, J. Phys. C 3, 285 (1970).

[49]G. C. Allen, J. A. Crofts, M. T. Curtis, P. M. Tucker, D. Chadwick, and P. J. Hampson, J. Chem. Soc. Dalton Trans. 1974, 1297.
[50]J. C. Fuggle and D. Menzel, Surf. Sci. 53, 21 (1975).
[51]J. C. Rivière, Brit. J. Appl. Phys. 15, 1341 (1964).
[52]D. Menzel, J. Vac. Sci. Technol. 12, 313 (1975).
[53]B. D. Padalia, J. K. Gimzewski, S. Affrossman, W. C. Lang, L. M. Watson, and D. J. Fabian, Surf. Sci. 61, 468 (1976).
[54]O. Gunnarsson and K. Schönhammer, Phys. Rev. Lett. 41, 1608 (1978).
[55]R. D. Mesmer and S. H. Lamson, Chem. Phys. Lett. 65, 465 (1979).
[56]P. R. Norton, R. L. Tapping, and J. W. Goodale, Surf. Sci. 72, 33 (1978).
[57]H. Hopster and C. R. Brundle, J. Vac. Sci. Technol. 16, 548 (1979).
[58]M. Breysse, B. Claudel, M. Prettre, and J. Veron, J. Catal. 24, 106 (1972).
[59]M. Breysse, B. Claudel, and J. Veron, Kinet. Katal. 14, 102 (1974).
[60]J. C. Fuggle, A. F. Burr, L. M. Watson, D. J. Fabian, and W. Lang, J. Phys. F 4, 335 (1973).
[61]C. D. Wagner, W. M. Riggs, L. E. Davis, and J. Moulder, *Handbook of X-Ray Photoelectron Spectroscopy* (Perkin Elmer Corp., Eden Prarie, MN, 1979).
[62]J. C. Fuggle and D. Menzel, Chem. Phys. Lett. 33, 37 (1975).
[63]J. C. Rivière, Brit. J. Appl. Phys. 16, 1507 (1965).
[64]R. W. Joyner, Surf. Sci. 63, 291 (1977).
[65]I. Barin, O. Knacke, and O. Kubaschewski, *Thermochemical Properties of Inorganic Substances* (Springer, New York, 1977).
[66]B. J. Hopkins, A. R. Jones, and R. I. Winton, Surf. Sci. 57, 226 (1976).
[67]L. R. Clavenna and L. D. Schmidt, Surf. Sci. 33, 11 (1972).